

## Size-Dependent Tunneling and Optical Spectroscopy of CdSe Quantum Rods

David Katz, Tommer Wizansky, and Oded Millo\*

*Racah Institute of Physics, and the Center for Nanoscience and Nanotechnology, The Hebrew University of Jerusalem, Jerusalem 91904, Israel*

Eli Rothenberg, Taleb Mokari, and Uri Banin†

*Institute of Chemistry, The Farkas Center for Light Induced Processes, and the Center for Nanoscience and Nanotechnology, The Hebrew University of Jerusalem, Jerusalem 91904, Israel*

(Received 25 April 2002; published 31 July 2002)

Photoluminescence excitation spectroscopy and scanning-tunneling spectroscopy are used to study the electronic states in CdSe quantum rods that manifest a transition from a zero-dimensional to a one-dimensional quantum-confined structure. Both optical and tunneling spectra show that the level structure depends primarily on the diameter of the rod and not its length. With increasing diameter, the band gap and the excited state level spacings shift to the red. The level structure was assigned using a multiband effective-mass model, showing a similar dependence on rod dimensions.

DOI: 10.1103/PhysRevLett.89.086801

PACS numbers: 73.22.-f, 73.63.-b, 78.67.-n

Colloidal semiconductor nanocrystals are a class of nanomaterials that manifest the transition from the molecular limit to the solid state [1,2], with significant potential for serving as building blocks of nanodevices in applications ranging from lasers [3,4] and optoelectronic devices [5] to biological fluorescence tagging [6]. Shape control of such colloiddally prepared nanostructures has recently been achieved by modifying the synthesis to obtain rod-shaped particles—quantum rods (QRs) [7]. QRs exhibit electronic and optical properties different from quantum dots (QDs). For example, unlike the spherical dots, QRs have linearly polarized emission as demonstrated recently by fluorescence measurements on single rods [8], and polarized lasing [4]. In this Letter we combine optical and tunneling spectroscopies to investigate the electronic level structure of CdSe quantum rods, and study its dependence on rod length and diameter. The levels are assigned with the use of a multiband effective-mass model. The study provides significant insight on the evolution of the electronic structure from zero-dimensional QDs to one-dimensional quantum wires.

The combination of scanning-tunneling and optical spectroscopies has proven to be a powerful approach to decipher the level structure of nanocrystal QDs [2,9]. While in the optical spectra, allowed valence band (VB) to conduction band (CB) transitions are detected [10,11], in tunneling spectroscopy the CB and VB states can be separately probed yielding complementary information on the level structure [9,12–14]. Such data provide an important test for theoretical models of the level structure in strongly quantum-confined nanostructures, as was demonstrated for spherical QDs [15,16]. Multiband effective-mass approaches [10,11,17] and atomistic pseudopotential theory [15] were both used to describe measured QD size-dependent level structure. The pseudopotential approach

was recently applied also for the calculation of energy levels in rods of small diameter and aspect ratios up to six [18].

The CdSe system studied here is highly developed synthetically, to a level where it serves as a model system for colloidal semiconductor nanostructures. Figure 1 presents transmission electron microscopy (TEM) images of typical samples of CdSe QRs grown using the well developed methods of colloidal nanocrystal synthesis, where the

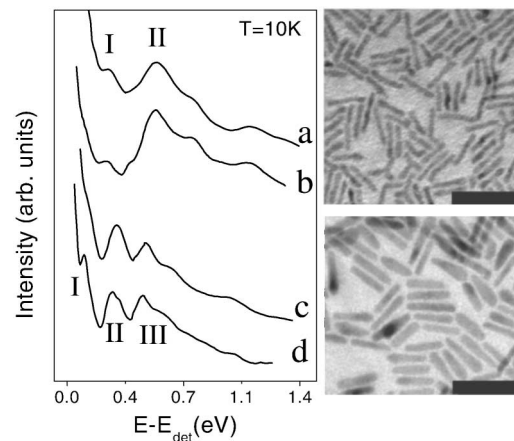


FIG. 1. PLE spectra for CdSe QRs are shown in the left frame (a)  $31 \times 1.9$  (length times radius) nm,  $E_{\text{det}} = 2.25$  eV; (b)  $11 \times 1.6$  nm,  $E_{\text{det}} = 2.25$  eV; (c)  $60 \times 3.3$  nm,  $E_{\text{det}} = 2.00$  eV; (d)  $11 \times 2.9$  nm,  $E_{\text{det}} = 2.03$  eV, with the zero energy representing the position of the detection window,  $E_{\text{det}}$ . Relevant optical transitions are marked. The structure above 0.7 eV is overlapping peaks of the excitation lamp that could not be completely normalized out. TEM images of two QR samples,  $31 \times 1.9$  nm (top), and  $30 \times 3.2$  nm (bottom), are shown to the right. Scale bar is 50 nm.

rods are overcoated by organic ligands [7,19,20]. For the study of length and diameter dependence we prepared six different samples with dimensions that can be divided into two groups: three samples with average radii  $\sim 1.8$  nm and lengths ranging from 11 to 31 nm, and three samples with radii  $\sim 3.2$  nm and lengths ranging from 11 to 60 nm. The spread of the rod dimensions, as determined from the TEM images, was 5% to 10% in diameter and 10%–15% in length. For the low temperature optical experiments, optically clear freestanding polymer films containing the rods were prepared. The cooled samples showed absorption spectra with several transitions and had a distinct photoluminescence (PL) peak assigned to band-gap emission. The positions of the absorption onset and PL peak redshifted with increasing diameter and showed no significant variation with rod length (see below) [21].

The photoluminescence excitation (PLE) spectra presented in Fig. 1, measured on four samples, were obtained by opening a narrow detection window at the blue edge of the inhomogeneously broadened PL peak [10,11]. The spectra are less structured as compared with those measured on QDs due to the increased sources of inhomogeneous broadening in rods and due to the intrinsically less discrete level structure. A striking feature is the nearly identical level structure observed for the two QR samples of small diameter [traces 1(a) and 1(b)], which differs significantly from the spectra measured on the thicker rods [traces 1(c) and 1(d)], although in each group the aspect ratios vary from three to about ten. This shows clearly that not only the band gap of the rods depends mainly on the diameter, but also the excited optical transitions.

The optical measurements were accompanied by scanning-tunneling microscopy (STM) measurements performed at 4.2 K on *single* QRs. The QRs were deposited on graphite by spin coating a dilute QR-hexane solution. A topographic image of a nanorod 25 nm in length and 2 nm in radius is presented in Fig. 2(a). The tunneling  $dI/dV$  vs  $V$  spectra were obtained in a double barrier tunnel junction (DBTJ) configuration [9,12–14], as shown schematically in Fig. 2(b). The spectra were measured with the tip retracted from the QR to a distance where the bias voltage is dropped largely across the tip-QR junction, and charging effects are avoided. As a result, CB (VB) states appear at positive (negative) sample bias, and the peak separations are close to the real QR level spacings. Moreover, as shown previously for QDs, the applied voltage does not affect much the level spectrum [16]. Hence, the  $dI/dV$  spectra yield direct information on the QR level structure [12–14].

The tunneling spectra in Fig. 2(c) further demonstrate, in accordance with the PLE data, that the QR level structure depends primarily on the diameter of the QRs, not on their length. Most significantly, the region of suppressed tunneling conductance (null density of states) around zero bias, associated with the quasiparticle energy gap, is redshifted upon QR thickening, from  $\sim 2.4$  eV in the upper two curves ( $r \sim 2$  nm) to  $\sim 2.2$  eV in the lower curves ( $r \sim 2.7$  nm). This trend was not observed as clearly for

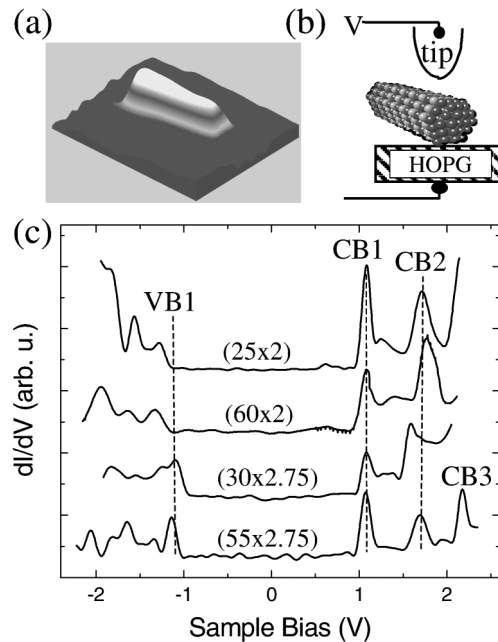


FIG. 2. (a) STM topographic image of a QR 25 nm long and 2 nm in radius (the apparent height is  $\sim 4.5$  nm). (b) Schematic of the DBTJ configuration used for acquiring the tunneling spectra. (c)  $dI/dV - V$  tunneling spectra for QRs of various lengths and radii, marked above each curve in nm. For clarity, the spectra were shifted horizontally to align the CB1 peaks. The vertical dashed lines are guides to the eye. The tunneling set values were in the range  $V_s = 1.5$ –2 V and  $I_s = 50$ –80 pA.

the spacing between the CB ground state (CB1) and the first excited state (CB2); see below. Level CB3, appearing in the lower trace, was observed in  $\sim 50\%$  of the measurements, where the current did not reach the saturation limit before resolving this level. The VB is considerably more dense and complex (see below), and its level structure was not reliably resolved in our tunneling spectra; we thus denote only the first (ground state) peak as VB1 [Fig. 2(c)]. More insight into the QR level structure, including the excited VB levels, is gained by correlating the tunneling spectra with allowed optical VB to CB transitions and comparing these data with model level-structure calculations.

To calculate the electronic structure of the rods we employ the formalism developed by Sercel and Vahala for quantum wires [22]. Similar basis functions were used for the envelope wave functions, with quantum numbers reflecting the cylindrical symmetry of the QR:  $n$ , the principal number (associated with the number of nodes along the radius), and  $F_z$  and  $L_z$ , the projections of the total and the envelope angular momenta along the  $z$  (symmetry) axis, respectively. Here  $F_z = J_z + L_z$ , where  $J_z$  is the projection of the band-edge Bloch angular momentum along the  $z$  axis. The finite length  $L$  of the QRs is expressed by introducing an additional quantum number, denoted by  $m$ , and a related factor,  $\exp(i\pi m z/L)$ , to the envelope wave functions, replacing the continuum wave vector  $K_z$  in Ref. [22].

We first consider the CB level structure. Here, due to the large band gap of CdSe (1.84 eV), the uncoupled one-band effective-mass model with quantum numbers  $(n, L_z, m)$  is adequate for rods of large enough aspect ratio [18,22]. Figure 3(a) presents CB energy levels calculated using this model for a particle in a finite cylindrical potential well ( $U = 5$  eV), as a function of radius and length (inset). The CB states with  $L_z = 0, 1,$  and  $2$  are denoted CB1, CB2, and CB3, respectively. This figure clearly depicts the strong dependence of the energy levels on the QR radius, due to the strong confinement associated with this “narrow dimension,” as opposed to the near lack of length dependence shown in the upper inset. The length dependence becomes significant only for small aspect ratio (around two), or for high  $m$  values, effectively shortening the QR, since the number of nodes along the  $z$  axis is  $m - 1$ , in agreement with Ref. [18].

The VB states were calculated using the four-band effective-mass model that couples heavy and light holes [22], where the quantum numbers are now  $(n, F_z, m)$ . Results of this calculation, performed for an infinite cylindrical potential well, are presented in Fig. 3(b), where states with  $F_z = 1/2, 3/2,$  and  $5/2$  (and  $m = 1$ ) are shown. Again, the near lack of dependence of the level structure on the rod length is manifested by the inset. It is evident that

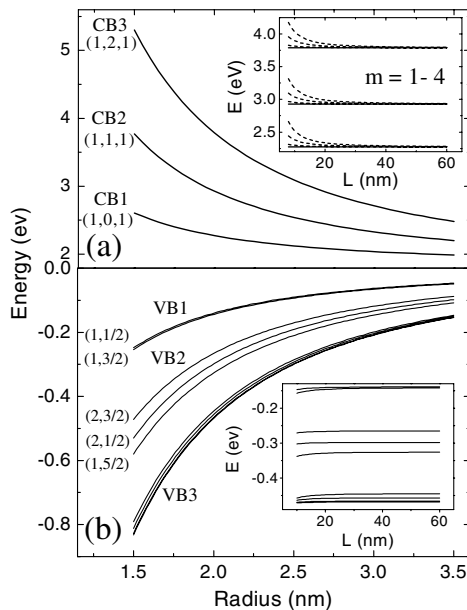


FIG. 3. Calculated energy levels of CdSe QRs. (a) First three CB states versus nanorod radius, for a 30 nm long QR. The quantum numbers  $(n, L_z, m)$  are denoted. (b) The VB energy levels versus QR radius calculated for a 30 nm long rod. The quantum numbers  $(n, F_z)$  are denoted ( $m = 1$ ). Group VB3 consists of states with  $F_z = 1/2, 3/2, 5/2,$  and  $7/2$ . Insets: Length dependence of the respective energy levels for a rod 2 nm in radius. The upper inset shows also the dependence on the  $m$  quantum number. The energies are given with respect to the bulk VB edge. Effective masses for electrons and holes and the bulk energy gap were taken from Ref. [17].

the VB is significantly more dense as compared to the CB. Yet, the VB levels near the band edge can be divided into three groups: VB1, denoting the two upper levels; VB2, the three subsequent ones; and VB3, the next group. Each of these groups is composed of various  $F_z$  levels, where, in turn, each  $F_z$  level has contributions from both heavy and light holes ( $J_z = 3/2$  and  $1/2$ , respectively), and thus from wave functions of different  $L_z$  values. This VB mixing leads to very weak selection rules for the optical transitions.

In Fig. 4 we compare the measured optical transitions and tunneling spectra with our theoretical calculations. The gap extracted from the optical measurements (solid circles) and the gap identified in the tunneling data (empty circles) are plotted in Fig. 4(a) along with the calculated energy gap, VB1-CB1. In order to compare with the quasiparticle (tunneling) gap, the measured excitonic (optical) gap was corrected for the electron-hole Coulomb interaction. As a first approximation, we modified the expression given in Ref. [10] for QDs,  $1.8e^2/kr$  (where  $k$  is the dielectric constant), to take into account the fact that in our QRs strong confinement holds only for the radial dimension. We thus replace the radius,  $r$ , by  $(r^2 a_0)^{1/3}$ , where  $a_0$  is the Bohr radius, 5.7 nm. A relatively good agreement between the calculated and measured energy gaps is found for both tunneling and optical experiments. However, the tunneling gaps are higher in energy and show a stronger dependence on radius as compared to the optical data, as was previously observed for QDs [9–11]. This can be ascribed to the nonvanishing voltage drop on the QR-substrate junction [12–14] and to the uncertainty involved in the determination of the QR radii [9]. Concerning the optical gap, the transition from both  $F_z = 1/2$  and  $3/2$  VB1 states are allowed. In the absorption they are too close to be resolved, but we note that the state with  $F_z = 1/2$  is the topmost state, from which theory predicts a transition polarized along the symmetry axis [23], consistent with PL polarization measurements for QRs [8].

Turning now to the excited levels, Fig. 4(b) shows spacings of the PLE transitions I and II with respect to the band-gap transition, together with levels CB2 and CB3 measured with respect to CB1, detected by tunneling. The data are presented as a function of the band gap measured in each experiment, thus eliminating the possible problem of QR radius estimation mentioned above. Most interesting is the good agreement of the spacing between PLE transition II and the band-gap transition (solid squares) with the tunneling data for the CB2-CB1 level separation (open squares), allowing a clear assignment of optical transition II. Both the optical and tunneling data correlate with the calculated CB2-CB1 spacing. It is also clear now that PLE transition I (solid stars) can take place only between an excited VB state and the CB ground state. However, due to the intricate VB level structure and the broad PLE features, it cannot be unambiguously assigned, and relatively good agreement is found for both calculated VB2-VB1 and VB3-VB1 level spacing (dashed lines). Transition III was

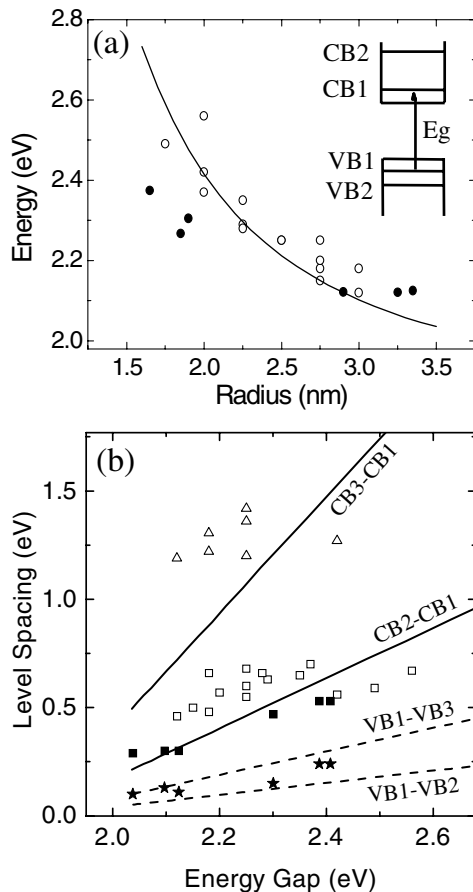


FIG. 4. (a) Energy gap versus QR radius. The tunneling data (empty circles, size digitized due to uncertainty) and the theory (solid line) represent the energy separations VB1-CB1. The optical data (solid circles) were determined from the first absorption peak and corrected for the electron-hole Coulomb interaction; see text. The inset illustrates the band-gap optical transition from VB1 to CB1. (b) Excited energy states versus energy gap. The calculated energy level separations, as denoted, are depicted by the solid and dashed lines. The respective separations between the tunneling peaks are denoted by open symbols. Spacing between PLE transitions I and II and the optical energy gap are presented by solid stars and squares, respectively. For the optical data, the energy gap was taken as the detection window corrected for the Coulomb interaction. The STM data represent 15 (out of 20) QRs whose spectra showed clear charging-free peak structure.

resolved only for the three samples with larger diameters, and thus cannot be assigned. Considering again the tunneling data, Fig. 4(b) shows a weaker size (energy-gap) dependence for CB2 and CB3 as compared to theory. This may be partly due to the perturbation of the tip-sample bias on the confining potential, which should affect mainly the higher levels.

The contribution of high  $m$  states was not clearly resolved in our spectra. In the PLE data, such a contribution possibly manifests itself in the broadening of the peaks, as compared with QDs. As for the tunneling spectra, due to the small wave vector component parallel to the surface

associated with the tunneling electron, coupling to higher  $m$  values may be suppressed. We note, however, that our spectra often exhibit a broad background on top of which the peaks are superimposed (e.g., the middle curves in Fig. 2).

In conclusion, optical and tunneling spectroscopic data for CdSe QRs show that the level structure is dominated by the radius rather than by the length. This behavior, manifested also in the theoretical calculations, reveals the quasi one-dimensional nature of the QR even for aspect ratios as small as three. This allows one to select a desired QR length and tune its optical or electrical properties at will, using the diameter. This ability is of significant importance for future nanotechnology applications of QRs [4,24].

This work was supported in part by the U.S.-Israel Binational Foundation, by the DIP Foundation, and by the Israel Science Foundation, Grants No. 99/00-12.5 and No. 8001/00-1.

\*Electronic address: milode@vms.huji.ac.il

†Electronic address: banin@chem.ch.huji.ac.il

- [1] A. P. Alivisatos, *Science* **271**, 933 (1996).
- [2] O. Millo, D. Katz, Y. W. Cao, and U. Banin, *Phys. Rev. Lett.* **86**, 5751 (2001).
- [3] V. Klimov *et al.*, *Science* **290**, 314 (2000).
- [4] M. Kazes *et al.*, *Adv. Mater.* **14**, 317 (2002).
- [5] N. Tessler, V. Medvedev, M. Kazes, S.H. Kan, and U. Banin, *Science* **295**, 1506 (2002).
- [6] M. Bruchez *et al.*, *Science* **281**, 1203 (1998).
- [7] X. G. Peng *et al.*, *Nature (London)* **404**, 59 (2000).
- [8] J. T. Hu *et al.*, *Science* **292**, 2060 (2001).
- [9] U. Banin, Y. W. Cao, D. Katz, and O. Millo, *Nature (London)* **400**, 542 (1999).
- [10] D. J. Norris and M. G. Bawendi, *Phys. Rev. B* **53**, 16338 (1996).
- [11] U. Banin *et al.*, *J. Chem. Phys.* **109**, 2306 (1998).
- [12] E. P. A. M. Bakkers and D. Vanmaekelbergh, *Phys. Rev. B* **62**, R7743 (2000).
- [13] E. P. A. M. Bakkers *et al.*, *Nano Lett.* **1**, 551 (2001).
- [14] D. Katz, O. Millo, S.H. Kan, and U. Banin, *Appl. Phys. Lett.* **79**, 117 (2001).
- [15] A. Franceschetti and A. Zunger, *Phys. Rev. B* **62**, 2614 (2000).
- [16] Y. M. Niquet *et al.*, *Phys. Rev. B* **65**, 165334 (2002).
- [17] A. I. Ekimov *et al.*, *J. Opt. Soc. Am. B* **10**, 100 (1993).
- [18] J. T. Hu *et al.*, *J. Phys. Chem.* **106**, 2447 (2002).
- [19] L. Manna, E. C. Scher, and A. P. Alivisatos, *J. Am. Chem. Soc.* **122**, 12700 (2000).
- [20] Z. A. Peng and X. Peng, *J. Am. Chem. Soc.* **123**, 1389 (2001).
- [21] L. S. Li, J. T. Hu, W. D. Yang, and A. P. Alivisatos, *Nano Lett.* **1**, 349 (2001).
- [22] P. C. Sercel and K. J. Vahala, *Phys. Rev. B* **42**, 3690 (1990).
- [23] P. C. Sercel and K. J. Vahala, *Phys. Rev. B* **44**, 5681 (1991).
- [24] W. U. Huynh, J. J. Dittmer, and A. P. Alivisatos, *Science* **295**, 2425 (2002).